SIAM/ASA J. Uncertainty Quantification
Vol. 4, pp. 1263–1287

Inverse Random Source Scattering Problems in Several Dimensions*

Gang Bao†, Chuchu Chen‡, and Peijun Li‡

Abstract. This paper concerns the source scattering problems for acoustic wave propagation, which is governed by the two- or three-dimensional stochastic Helmholtz equation. As a source, the electric current density is assumed to be a random function driven by an additive colored noise. Given the random source, the direct problem is to determine the radiated random wave field. The inverse problem is to reconstruct statistical properties of the source from the boundary measurement of the radiated random wave field. In this work, we consider both the direct and inverse problems. We show that the direct problem has a unique mild solution via a constructive proof. Using the mild solution, we derive effective Fredholm integral equations for the inverse problem. A regularized Kaczmarz method is developed by adopting multifrequency scattering data to overcome the challenges of solving the ill-posed and large scale integral equations. Numerical experiments are presented to demonstrate the efficiency of the proposed method. The framework and methodology developed here are expected to be applicable to a wide range of stochastic inverse source problems.

Key words. inverse source scattering problem, stochastic differential equations, Fredholm integral equations

AMS subject classifications. 78A46, 65C30

DOI. 10.1137/16M1067470

1. Introduction.

Motivated by significant scientific and industrial applications, the field of inverse problems has undergone tremendous growth in the last several decades since Calderón proposed an inverse conductivity problem [11]. In particular, inverse scattering problems have progressed to an area of intense activity and are currently in the foreground of mathematical research in scattering theory [14]. As an important example, the inverse source scattering problem is to determine the unknown source that generates a prescribed radiated wave pattern. It is motivated by medical applications where it is desirable to use electric or magnetic measurements on the surface of the human body, such as the head, to infer the source currents inside of the body, such as the brain, that produced these measured data [21, 25]. It has been considered as a basic tool for the solution of reflection tomography and diffusive optical tomography.

The inverse source scattering problem has been investigated extensively in the literature. There is a lot of information available concerning its solution mathematically and numerically

*Received by the editors March 23, 2016; accepted for publication (in revised form) August 29, 2016; published electronically October 27, 2016.

http://www.siam.org/journals/juq/4/M106747.html

Funding: The research of the first author was supported in part by a Key Project of the Major Research Plan of NSFC (91130004), an NSFC A3 project (11421110002), NSFC Tianyuan projects (11426235, 11526211), and a special research grant from Zhejiang University. The research of the second author was partially supported by the National Natural Science Foundation of China (91130003, 11021101, and 11290142). The research of the third author was partially supported by the NSF DMS-1151308.

†School of Mathematical Sciences, Zhejiang University, Hangzhou 310027, China (baog@zju.edu.cn).

‡Department of Mathematics, Purdue University, West Lafayette, IN 47907 (chen2095@math.purdue.edu, lipeijun@math.purdue.edu).

[2, 3, 4, 17, 19, 28, 33]. For instance, there exist an infinite number of sources that radiate fields which vanish identically outside their supported domain so that the inverse source problem does not have a unique solution at a fixed frequency [18, 23]. More challenging, it is ill-posed as small variations in the measured data can lead to huge errors in the reconstructions. To overcome these obstacles, one may either seek the minimum energy solution, which represents the pseudoinverse of the problem, or use multifrequency scattering data to ensure uniqueness and gain increased stability of the solution [7, 8, 9].

Stochastic inverse problems refer to inverse problems that involve uncertainties, which are widely introduced into the mathematical models for three major reasons: randomness may directly appear in the studied systems [20], incomplete knowledge of the systems must be modeled by uncertainties [26], and stochastic techniques are introduced to couple the large scale span [30]. They are commonly encountered and can happen simultaneously for many different problems [22]. Compared with classical inverse problems, stochastic inverse problems have substantially more difficulties due to the randomness. Unlike the deterministic nature of solutions for classical inverse problems, solutions for stochastic inverse problems are random functions. It is less meaningful to find a solution for a particular realization of the randomness. The statistics, such as mean, variance, and even higher order moments, of the solution are more desirable.

The inverse random source scattering problem is used to determine statistical structures of the source from boundary measurements of the radiated fields. This is an important problem that arises, e.g., in fluorescence microscopy [32], where the randomly distributed fluorescence in the specimen (such as green fluorescent protein) gives rise to emitted light which is focused to the detector by the same objective that is used for the excitation. It is desirable to model the fluorescence light source as a random function. Although the deterministic counterpart has been well studied, little is known for the stochastic case [16]. Recently, some one-dimensional stochastic inverse source problems were considered in [6, 10, 27], where the governing equations are stochastic ordinary differential equations. Unfortunately, these approaches could not be extended directly to the multidimensional problem.

In this paper, we study both the direct and inverse source scattering problems for the two- or three-dimensional stochastic Helmholtz equation. As a source, the electric current density is assumed to be a random function driven by a colored noise which includes the white noise when the correlation function is the delta function. Given the source, the direct problem is to determine the random wave field. The inverse problem is to reconstruct the mean and variance of the random source by using the same statistics of the radiated fields, which are measured on a boundary enclosing the compactly supported source at multiple frequencies. By constructing a sequence of regular processes approximating the colored noise, we show that there exists a unique mild solution to the stochastic direct scattering problem. By examining the expectation and variance of the mild solution, we derive Fredholm integral equations to solve the inverse problem for the white noise. It is known that Fredholm integral equations of the first kind are severely ill-posed, which can be clearly seen from the distribution of singular values for our integral equations. It is particularly true for the integral equations of reconstructing the variance. To overcome the challenges of the ill-posed and large scale integral equations, we propose equations with better conditioning via linear combination of the original equations and develop a regularized Kaczmarz method to solve the resulting linear

system of algebraic equations. The method is consistent with the data nature and requires solving a relatively small scale system at each iteration. Numerical experiments show that the proposed method is effective for solving both the two- and three-dimensional problems.

This paper presents the first approach for solving the stochastic inverse source scattering problem in higher dimensions. Apparently, the techniques differ greatly from the existing one-dimensional work [6, 27] because we need to consider more complicated stochastic partial differential equations instead of stochastic ordinary differential equations. The proposed framework and methodology can be directly applied to solving many other inverse random source problems of stochastic differential equations such as the Poisson equation, the heat equation, and the wave equation. It also has great potential to be applicable to more general stochastic inverse problems.

The outline of this paper is as follows. In section 2, we introduce the stochastic Helmholtz equation and discuss the solutions for the deterministic and stochastic problems. Section 3 is devoted to the inverse problem, where Fredholm integral equations are deduced and the regularized Kaczmarz method is developed to reconstruct the mean and the variance. Numerical experiments are presented in section 4 to illustrate the performance of the proposed method. The paper is concluded with general remarks and directions for current and future research in section 5.

2. Direct problem.

In this section, we introduce the Helmholtz equation and discuss the solutions of the deterministic and stochastic direct source scattering problems.

2.1. Problem formulation.

Consider the scattering problem of the Helmholtz equation in a homogeneous medium

$$\Delta u + \kappa^2 u = f \quad \text{in } \mathbb{R}^d, \tag{2.1}$$

where $d = 2$ or 3, the wavenumber $\kappa > 0$ is a constant, the electric current density f is assumed to be a random function driven by an additive noise

$$f(x) = g(x) + \sigma(x)\dot{W}_x, \tag{2.2}$$

and u is the radiated random wave field. Here g and $\sigma \geq 0$ are two deterministic real functions which have compact supports contained in the rectangular domain $D \subset \mathbb{R}^d$, and $\dot{W}_x$ is a homogeneous colored noise. To make the paper self-contained, some preliminaries are presented in the appendix for the Brownian sheet, white noise, colored noise, and corresponding stochastic integrals. More details can be found in [15, 31] on an introduction to stochastic differential equations. The Sommerfeld radiation condition is required for the radiated wave field,

$$\lim_{r\to\infty} r^{\frac{d-1}{2}}(\partial_r u - \mathrm{i}\kappa u) = 0, \quad r = |x|, \tag{2.3}$$

uniformly in all directions $\hat{x} = x/|x|$.

Denote by $B_\rho(y)$ the ball with radius ρ and center at y, i.e., $B_\rho(y) = \{x \in \mathbb{R}^d : |x-y| < \rho\}$. Let $B_\rho = B_\rho(0)$ if the center is at the origin. Let $R > 0$ be large enough such that $\bar{D} \subset B_R$. Denote by ∂B_R the boundary of B_R. Given the random electric current density function

f, the direct problem is to determine the random wave field u of the stochastic scattering problem (2.1), (2.3). The inverse problem is to reconstruct g and σ^2 from the measured wave field on ∂B_R at a finite number of wavenumbers $\kappa_j, j = 1, \ldots, m$.

2.2. Deterministic direct problem. We begin with the solution for the deterministic direct problem. Let $\sigma = 0$ in (2.2), i.e., no randomness is present in the source. The stochastic scattering problem (2.1), (2.3) reduces to the deterministic scattering problem:

$$\begin{cases} \Delta u + \kappa^2 u = g & \text{in } \mathbb{R}^d, \\ \partial_r u - \mathrm{i}\kappa u = o(r^{-\frac{d-1}{2}}) & \text{as } r \to \infty. \end{cases} \tag{2.4}$$

Given $g \in L^2(D)$, it is known that the scattering problem (2.4) has a unique solution

$$u(x) = \int_D G(x, y) g(y) \mathrm{d}y, \tag{2.5}$$

where G is Green's function of the Helmholtz equation. Explicitly, we have

$$G(x, y) = \begin{cases} G_2(x, y) = -\dfrac{\mathrm{i}}{4} H_0^{(1)}(\kappa|x - y|), & d = 2, \\ G_3(x, y) = -\dfrac{1}{4\pi} \dfrac{e^{\mathrm{i}\kappa|x-y|}}{|x - y|}, & d = 3. \end{cases}$$

The following regularity results of Green's function play an important role in the subsequent analysis.

Lemma 2.1. *Let $\Omega \subset \mathbb{R}^d$ be a bounded domain. It holds that $G(x, y) \in L^2(\Omega)$ for any $y \in \Omega$.*

Proof. Let $\rho = \sup_{x,y\in\Omega} |x - y|$. We have $\bar{\Omega} \subset B_\rho(y)$. It is known for $d = 2$ that

$$G_2(x, y) = -\frac{1}{2\pi} \log \frac{1}{|x - y|} + V(x, y),$$

where V is a Lipschitz continuous function. Hence, it suffices to show that

$$\log \frac{1}{|x - y|} \in L^2(\Omega) \quad \text{for any } y \in \Omega.$$

A simple calculation yields

$$\int_\Omega \left| \log \frac{1}{|x - y|} \right|^2 \mathrm{d}x \le \int_{B_\rho(y)} \left| \log \frac{1}{|x - y|} \right|^2 \mathrm{d}x \lesssim \int_0^\rho r \left| \log \frac{1}{r} \right|^2 \mathrm{d}r < \infty.$$

For $d = 3$, we have

$$\int_\Omega |G_3(x, y)|^2 \mathrm{d}x \lesssim \int_{B_\rho(y)} \frac{1}{|x - y|^2} \mathrm{d}x \lesssim \int_0^\rho \mathrm{d}r < \infty,$$

which completes the proof. ∎

Throughout the paper, $a \lesssim b$ stands for $a \le Cb$, where $C > 0$ is a constant. The specific value of C is not required but should be clear from the context.

Lemma 2.2. *Let $\Omega \subset \mathbb{R}^d$ be a bounded domain.*

1. *When $d = 2$, it holds for any $\alpha \in (\frac{3}{2}, \infty)$ that*

$$\int_\Omega |G_2(x,y) - G_2(x,z)|^\alpha \mathrm{d}x \lesssim |y-z|^{\frac{3}{2}} \quad \text{for any } y, z \in \Omega. \tag{2.6}$$

2. *When $d = 3$, it holds for any $\beta \in (1, 3)$ and $\gamma = \min\{3-\beta, \beta\}$ that*

$$\int_\Omega |G_3(x,y) - G_3(x,z)|^\beta \mathrm{d}x \lesssim |y-z|^{\gamma} \quad \text{for any } y, z \in \Omega. \tag{2.7}$$

Proof. Here we only present the proof of (2.6) since the proof of (2.7) can be found in [12]. Similarly, it suffices to show (2.6) for the singular part of G_2. A simple calculation yields

$$\begin{aligned}
&\int_\Omega \left| \log \frac{1}{|x-y|} - \log \frac{1}{|x-z|} \right|^\alpha \mathrm{d}x \\
&= \int_\Omega \left(\frac{1}{|x-y|} - \frac{1}{|x-z|} \right)^{\frac{3}{2}} \left| \log \frac{1}{|x-y|} - \log \frac{1}{|x-z|} \right|^{\alpha-\frac{3}{2}} \\
&\quad \times \left(\int_0^1 \left(\frac{t}{|x-y|} + \frac{1-t}{|x-z|} \right)^{-1} \mathrm{d}t \right)^{\frac{3}{2}} \mathrm{d}x \\
&\le \int_\Omega \frac{|y-z|^{\frac{3}{2}}}{|x-y|^{\frac{3}{2}}|x-z|^{\frac{3}{2}}} \left| \log \frac{1}{|x-y|} - \log \frac{1}{|x-z|} \right|^{\alpha-\frac{3}{2}} \\
&\quad \times \left(\int_0^1 \left(\frac{t}{|x-y|} + \frac{1-t}{|x-z|} \right)^{-1} \mathrm{d}t \right)^{\frac{3}{2}} \mathrm{d}x \\
&\le |y-z|^{\frac{3}{2}} \int_\Omega \frac{(|x-y| + |x-z|)^{\frac{3}{2}}}{|x-y|^{\frac{3}{2}}|x-z|^{\frac{3}{2}}} \left| \log \frac{1}{|x-y|} - \log \frac{1}{|x-z|} \right|^{\alpha-\frac{3}{2}} \mathrm{d}x \\
&\le |y-z|^{\frac{3}{2}} \int_\Omega \left(\frac{1}{|x-y|^{\frac{3}{2}}} + \frac{1}{|x-z|^{\frac{3}{2}}} \right) \left| \log \frac{1}{|x-y|} - \log \frac{1}{|x-z|} \right|^{\alpha-\frac{3}{2}} \mathrm{d}x,
\end{aligned}$$

where in the second inequality we have utilized the estimate $\forall\, t \in [0,1]$,

$$w(t) = \left(\frac{t}{|x-y|} + \frac{1-t}{|x-z|} \right)^{-1} \le \max\{w(0), w(1)\} < w(0) + w(1) = |x-y| + |x-z|.$$

Using the Hölder inequality, we get that

$$\begin{aligned}
&\int_\Omega \left| \log \frac{1}{|x-y|} - \log \frac{1}{|x-z|} \right|^\alpha \mathrm{d}x \\
&\le |y-z|^{\frac{3}{2}} \left(\int_\Omega \left(\frac{1}{|x-y|^{\frac{3}{2}}} + \frac{1}{|x-z|^{\frac{3}{2}}} \right)^{\frac{6}{5}} \mathrm{d}x \right)^{\frac{5}{6}} \\
&\quad \times \left(\int_\Omega \left| \log \frac{1}{|x-y|} - \log \frac{1}{|x-z|} \right|^{6\alpha-9} \mathrm{d}x \right)^{\frac{1}{6}}.
\end{aligned}$$

Let $\rho = \sup_{x,y\in\Omega} |x-y|$. We have $\bar{\Omega} \subset B_\rho(y)$ and $\bar{\Omega} \subset B_\rho(z)$. It is easy to verify that

$$\begin{aligned}\int_\Omega \left(\frac{1}{|x-y|^{\frac{3}{2}}} + \frac{1}{|x-z|^{\frac{3}{2}}} \right)^{\frac{6}{5}} \mathrm{d}x &\lesssim \int_{B_\rho(y)} \frac{1}{|x-y|^{\frac{9}{5}}} \mathrm{d}x + \int_{B_\rho(z)} \frac{1}{|x-z|^{\frac{9}{5}}} \mathrm{d}x \\ &\lesssim \int_0^\rho r^{-\frac{4}{5}} \mathrm{d}r + \int_0^\rho r^{-\frac{4}{5}} \mathrm{d}r < \infty\end{aligned}$$

and

$$\begin{aligned}&\int_\Omega \left| \log \frac{1}{|x-y|} - \log \frac{1}{|x-z|} \right|^{6\alpha-9} \mathrm{d}x \\ \lesssim &\int_{B_\rho(y)} \left| \log \frac{1}{|x-y|} \right|^{6\alpha-9} \mathrm{d}x + \int_{B_\rho(z)} \left| \log \frac{1}{|x-z|} \right|^{6\alpha-9} \mathrm{d}x \\ \lesssim &\int_0^\rho r \left| \log \frac{1}{r} \right|^{6\alpha-9} \mathrm{d}r + \int_0^\rho r \left| \log \frac{1}{r} \right|^{6\alpha-9} \mathrm{d}r < \infty.\end{aligned}$$

Combining the above estimates completes the proof. ∎

2.3. Stochastic direct problem. In this section, we discuss the solution for the stochastic direct source problem (2.1), (2.3). Consider the scattering problem

$$\begin{cases} \Delta u + \kappa^2 u = g + \sigma \dot{W}_x & \text{in } \mathbb{R}^d, \\ \partial_r u - \mathrm{i}\kappa u = o(r^{-\frac{d-1}{2}}) & \text{as } r \to \infty, \end{cases} \tag{2.8}$$

where the homogeneous colored noise $\dot{W}_x$ has a correlation function

$$c(x,y) = \mathbf{E}(\dot{W}_x \dot{W}_y) = c(x-y) \quad \text{for any } x, y \in \mathbb{R}^d.$$

We assume that $c \in L^{q_0}_{\mathrm{loc}}(\mathbb{R}^d)$ for some $q_0 \geq 1$.

Remark 2.3. In practice, there are three types of commonly used correlation functions.

1. Delta kernel: if $c(x) = \delta(x)$, then $q_0 = 1$ and the colored noise reduces to the white noise.
2. Riesz kernel: if $c(x) = |x|^{-\nu}, 0 < \nu < d$. Let $\Omega \subset \mathbb{R}^d$ be a compact set and take $\rho > 0$ to be sufficiently large such that $\bar{\Omega} \subset B_\rho$. It is easy to show that $q_0 \in [1, \frac{d}{\nu})$ since

$$\|c\|^{q_0}_{L^{q_0}(\Omega)} \leq \int_{B_\rho(0)} |x|^{-\nu q_0} \mathrm{d}x \leq \int_0^\rho r^{d-1} r^{-\nu q_0} \mathrm{d}r < \infty$$

   if $d - 1 - \nu q_0 > -1$, i.e., $q_0 < \frac{d}{\nu}$.
3. Heat kernel: if $c(x) = e^{-|x|^2}$. It is clear to note that $q_0 \in [1, \infty]$.

We make the following hypothesis on the coefficients g and σ to support the well-posedness of the solution (2.8).

Hypothesis 2.4. *Assume that $g \in L^2(D)$ and $\sigma \in L^p(D)$, where $p \in (p_0, \infty]$ if $\frac{3}{2} \le p_0 \le 2$, or $p \in (p_0, \frac{3p_0}{3-2p_0})$ if $1 \le p_0 < \frac{3}{2}$ for $d = 2$, and $p \in (\frac{3p_0}{3-p_0}, \infty]$ for $d = 3$. Moreover, we require that $\sigma \in C^{0,\eta}(D)$, i.e., η-Hölder continuous, where $\eta \in (0, 1]$.*

Under Hypothesis 2.4, we may show that the unique solution of (2.8) is given by

$$u(x) = \int_D G(x, y)g(y)\mathrm{d}y + \int_D G(x, y)\sigma(y)\mathrm{d}W_y.$$

Before discussing the solution of the stochastic scattering problem (2.8), let us first make some comments about Hypothesis 2.4. The assumption on $g \in L^2(D)$ is motivated by the solution of the deterministic direct problem (2.4). The regularity of σ is chosen such that the stochastic integral

$$\int_D G(x, y)\sigma(y)\mathrm{d}W_y$$

is well-posed, i.e., it satisfies

$$\begin{aligned} &\mathbf{E}\left(\left|\int_D G(x, y)\sigma(y)\mathrm{d}W_y\right|^2\right) \\ &= \int_D \int_D G(x, y)\sigma(y)c(y - z)\overline{G}(x, z)\sigma(z)\mathrm{d}y\mathrm{d}z < \infty, \end{aligned} \tag{2.9}$$

where Proposition B.1 is used in the above identity.

We will need the following Young's inequality for convolutions (cf. [1, Theorem 2.24]).

Lemma 2.5. *Let $p, q, r \ge 1$ and suppose that $\frac{1}{p} + \frac{1}{q} + \frac{1}{r} = 2$. It holds that*

$$\left|\int_{\mathbb{R}^d} \int_{\mathbb{R}^d} u(x)v(x - y)w(y)\mathrm{d}x\mathrm{d}y\right| \le \|u\|_p\|v\|_q\|w\|_r$$

$\forall u \in L^p(\mathbb{R}^d), v \in L^q(\mathbb{R}^d), w \in L^r(\mathbb{R}^d)$.

Applying Lemma 2.5 to the integral in the right-hand side of (2.9) leads to

$$\begin{aligned} &\int_D \int_D G(x, y)\sigma(y)c(y - z)\overline{G}(x, z)\sigma(z)\mathrm{d}y\mathrm{d}z \\ &= \int_{\mathbb{R}^d} \int_{\mathbb{R}^d} \chi_D(y)G(x, y)\sigma(y)\chi_{B_{2R}}(y - z)c(y - z)\chi_D(z)\overline{G}(x, z)\sigma(z)\mathrm{d}y\mathrm{d}z \\ &\le \|G(x, \cdot)\sigma(\cdot)\|^2_{L^{p_0}(D)}\|c\|_{L^{q_0}(B_{2R})}, \end{aligned}$$

where $p_0 = \frac{2q_0}{2q_0-1}$. Note that from $q_0 \ge 1$, we have $p_0 \in [1, 2]$.

Remark 2.6. For the delta kernel, it is easy to verify that

$$\mathbf{E}\left(\left|\int_D G(x, y)\sigma(y)\mathrm{d}W_y\right|^2\right) = \int_D |G(x, y)|^2\sigma^2(y)\mathrm{d}y.$$

Hence we require that $p_0 = 2$. In fact, when $c(x) = \delta(x)$ and $q_0 = 1$, we have $p_0 = \frac{2q_0}{2q_0-1} = 2$.

When $d = 2$, we consider the singular part of Green's function. It follows from the Hölder inequality that

$$\int_D \left|\log\frac{1}{|x-y|}\right|^{p_0}\sigma^{p_0}(y)\mathrm{d}y \le \left(\int_D \left|\log\frac{1}{|x-y|}\right|^{\frac{p_0 p}{p-p_0}}\mathrm{d}y\right)^{\frac{p-p_0}{p}}\left(\int_D |\sigma(y)|^p\mathrm{d}y\right)^{\frac{p_0}{p}}.$$

Since the first term on the right-hand side of the above inequality is a singular integral, p should be chosen such that it is well defined. Let $\rho > 0$ be sufficiently large such that $\bar{D} \subset B_\rho(x)$. A simple calculation yields

$$\int_D \left|\log\frac{1}{|x-y|}\right|^{\frac{p_0 p}{p-p_0}}\mathrm{d}y \le \int_{B_\rho(x)} \left|\log\frac{1}{|x-y|}\right|^{\frac{p_0 p}{p-p_0}}\mathrm{d}y \lesssim \int_0^\rho r\left|\log\frac{1}{r}\right|^{\frac{p_0 p}{p-p_0}}\mathrm{d}r.$$

It is clear to note that the above integral is well defined when $p > p_0$.

Besides, we require that $\frac{p_0 p}{p-p_0} > \frac{3}{2}$ in order to utilize (2.6), which means that if $1 \le p_0 < \frac{3}{2}$, then we need $p \in (p_0, \frac{3p_0}{3-2p_0})$; else if $\frac{3}{2} \le p_0 \le 2$, then we only need $p > p_0$.

When $d = 3$, we have from the Hölder inequality that

$$\begin{aligned}\int_D |G_3(x,y)|^{p_0}\sigma^{p_0}(y)\mathrm{d}y &\lesssim \int_D |x-y|^{-p_0}\sigma^{p_0}(y)\mathrm{d}y \\ &\le \left(\int_D |x-y|^{-\frac{p_0 p}{p-p_0}}\mathrm{d}y\right)^{\frac{p-p_0}{p}}\left(\int_D |\sigma(y)|^p\mathrm{d}y\right)^{\frac{p_0}{p}}.\end{aligned}$$

Similarly, we may pick a ball $B_\rho(x)$ satisfying $\bar{D} \subset B_\rho(x)$ such that

$$\int_D |x-y|^{-\frac{p_0 p}{p-p_0}}\mathrm{d}y \le \int_{B_\rho(x)} |x-y|^{-\frac{p_0 p}{p-p_0}}\mathrm{d}y \lesssim \int_0^\rho r^{-\left(\frac{p_0 p}{p-p_0}-2\right)}\mathrm{d}r.$$

Clearly, the above integral is well defined when $\frac{p_0 p}{p-p_0} - 2 < 1$, which gives $p > \frac{3p_0}{3-p_0}$. Therefore we conclude that $p > \frac{3p_0}{3-p_0}$ for $d = 3$.

Finally note that the Hölder continuity will be used in the analysis for existence of the solution.

Now we are in the position to present the well-posedness of the solution for the stochastic scattering problem (2.8). The explicit solution will be used to derive Fredholm integral equations for the inverse problem.

Theorem 2.7. *Let $\Omega \subset \mathbb{R}^d$ be a bounded domain. Under Hypothesis 2.4, there exists a unique continuous stochastic process $u : \Omega \to \mathbb{C}$ satisfying*

$$u(x) = \int_D G(x,y)g(y)\mathrm{d}y + \int_D G(x,y)\sigma(y)\mathrm{d}W_y, \tag{2.10}$$

which is called the mild solution of the stochastic scattering problem (2.8).

Proof. First we show that there exists a continuous modification of the random field

$$v(x) = \int_D G(x,y)\sigma(y)\mathrm{d}W_y, \quad x \in \Omega.$$

For any $x, z \in \Omega$, we have from Proposition B.1, Lemma 2.5, and the Hölder inequality that

$$\begin{aligned}\mathbf{E}(|v(x)-v(z)|^2) &= \int_D\int_D \left(G(x,y)-G(z,y)\right)\sigma(y)\\ &\quad\times c(y-\xi)\left(\overline{G}(x,\xi)-\overline{G}(z,\xi)\right)\sigma(\xi)\mathrm{d}y\mathrm{d}\xi\\ &\le \|\left(G(x,\cdot)-G(z,\cdot)\right)\sigma(\cdot)\|^2_{L^{p_0}(D)}\|c\|_{L^{q_0}(B_{2R})}\\ &\le \|G(x,\cdot)-G(z,\cdot)\|^2_{L^{\frac{p_0p}{p-p_0}}(D)}\|\sigma\|^2_{L^p(D)}\|c\|_{L^{q_0}(B_{2R})}.\end{aligned}$$

When $d=2$ and $\frac{p_0p}{p-p_0} > \frac{3}{2}$, it follows from (2.6) that

$$\int_D |G_2(x,y)-G_2(z,y)|^{\frac{p_0p}{p-p_0}}\mathrm{d}y \lesssim |x-z|^{\frac{3}{2}},$$

which gives

$$\mathbf{E}(|v(x)-v(z)|^2) \lesssim |x-z|^{\frac{3(p-p_0)}{p_0p}}.$$

Since $v(x)-v(z)$ is a random Gaussian variable, we have (cf. [24, Proposition 3.14]) for any integer q that

$$\mathbf{E}(|v(x)-v(z)|^{2q}) \lesssim (\mathbf{E}(|v(x)-v(z)|))^{2q} \le \left(\mathbf{E}(|v(x)-v(z)|^2)\right)^q \lesssim |x-z|^{\frac{3q(p-p_0)}{p_0p}}.$$

Taking $q > \frac{p_0p}{3(p-p_0)}$, we obtain from Kolmogorov's continuity theorem that there exists a continuous modification of the random field v.

When $d=3$ and $\frac{p_0p}{p-p_0} < 3$, we know from (2.7) that

$$\int_D |G_3(x,y)-G_3(x,z)|^{\frac{p_0p}{p-p_0}}\mathrm{d}y \lesssim |x-z|^{\gamma}$$

with $\gamma = \min\{\frac{p_0p}{p-p_0}, 3-\frac{p_0p}{p-p_0}\}$, which gives

$$\mathbf{E}(|v(x)-v(z)|^2) \lesssim |x-z|^{\frac{2\gamma(p-p_0)}{p_0p}}.$$

Similarly, we get for any integer q that

$$\mathbf{E}(|v(x)-v(z)|^{2q}) \lesssim |x-z|^{\frac{2q\gamma(p-p_0)}{p_0p}}.$$

Taking $q > \frac{p_0p}{2\gamma(p-p_0)}$ and using Kolmogorov's continuity theorem, we obtain that there exists a continuous modification of the random field v.

Clearly, the uniqueness of the mild solution comes from the solution representation (2.10), which depends only on the Green function G and the source functions g and σ.

Next we present a constructive proof to show the existence. We shall construct a sequence of processes $\dot{W}_x^n$ satisfying $\sigma\dot{W}^n \in L^2(D)$ and a sequence

$$v^n(x) = \int_D G(x,y)\sigma(y)\mathrm{d}W_y^n, \quad x \in \Omega,$$

which satisfies $v^n \to v$ in $L^2(\Omega)$ as $n \to \infty$.

Let $\mathcal{T}_n = \cup_{j=1}^n K_j$ be a regular triangulation of D, where K_j are either triangles for $d = 2$ or tetrahedra for $d = 3$. The piecewise constant approximation sequence is given by

$$\dot{W}_x^n = \sum_{j=1}^n |K_j|^{-1} \int_{K_j} \mathrm{d}W_x \chi_j(x),$$

where χ_j is the characteristic function of K_j and

$$\int_{K_j} \mathrm{d}W_x \sim \mathcal{N}(0, \mathrm{Var}_j), \quad \mathrm{Var}_j = \int_{K_j}\int_{K_j} c(x-y)\mathrm{d}x\mathrm{d}y.$$

Clearly we have for any $p \geq 1$ that

$$\begin{aligned}
\mathbf{E}\left(\|\dot{W}^n\|_{L^p(D)}^p\right) &= \mathbf{E}\left(\int_D \left|\sum_{j=1}^n |K_j|^{-1}\int_{K_j} \mathrm{d}W_x\chi_j(x)\right|^p \mathrm{d}x\right) \\
&\lesssim \mathbf{E}\left(\int_D \sum_{j=1}^n |K_j|^{-p}\left|\int_{K_j}\mathrm{d}W_x\right|^p \chi_j(x)\mathrm{d}x\right) \lesssim \sum_{j=1}^n |K_j|^{1-p}(\mathrm{Var}_j)^{\frac{p}{2}} < \infty,
\end{aligned}$$

which shows that $\dot{W}^n \in L^p(D)$, for any $p \geq 1$. It follows from the Hölder inequality that for a given p meeting Hypothesis 2.4, we let q satisfying $\frac{1}{p} + \frac{1}{q} = \frac{1}{2}$, and then

$$\|\sigma\dot{W}^n\|_{L^2(D)} \lesssim \|\sigma\|_{L^p(D)}^2 \|\dot{W}^n\|_{L^q(D)}^2 < \infty,$$

which means $\sigma\dot{W}^n \in L^2(D)$.

Using Proposition B.1 and Lemma 2.5, we have

$$\begin{aligned}
&\mathbf{E}\left(\int_\Omega \left|\int_D G(x,y)\sigma(y)\mathrm{d}W_y - \int_D G(x,y)\sigma(y)\mathrm{d}W_y^n\right|^2 \mathrm{d}x\right) \\
&= \mathbf{E}\left(\int_\Omega \left|\sum_{j=1}^n \int_{K_j} G(x,y)\sigma(y)\mathrm{d}W_y - \sum_{j=1}^n |K_j|^{-1}\int_{K_j} G(x,z)\sigma(z)\mathrm{d}z\int_{K_j}\mathrm{d}W_y\right|^2 \mathrm{d}x\right) \\
&= \mathbf{E}\left(\int_\Omega \left|\sum_{j=1}^n \int_{K_j}\int_{K_j} |K_j|^{-1}(G(x,y)\sigma(y) - G(x,z)\sigma(z))\mathrm{d}z\mathrm{d}W_y\right|^2 \mathrm{d}x\right)
\end{aligned}$$

$$= \mathbf{E}\left[\int_\Omega \left|\int_D \sum_{j=1}^n \chi_j(y)|K_j|^{-1}\int_{K_j}(G(x,y)\sigma(y)-G(x,z)\sigma(z))\mathrm{d}z\mathrm{d}W_y\right|^2 \mathrm{d}x\right]$$

$$\le \int_\Omega \left\|\sum_{j=1}^n \chi_j(\cdot)|K_j|^{-1}\int_{K_j}(G(x,\cdot)\sigma(\cdot)-G(x,z)\sigma(z))\mathrm{d}z\right\|^2_{L^{p_0}(D)} \|c\|_{L^{q_0}(B_{2R})}\mathrm{d}x.$$

Since

$$\left\|\sum_{j=1}^n \chi_j(\cdot)|K_j|^{-1}\int_{K_j}(G(x,\cdot)\sigma(\cdot)-G(x,z)\sigma(z))\mathrm{d}z\right\|^2_{L^{p_0}(D)}$$

$$= \left[\int_D \left|\sum_{j=1}^n \chi_j(y)|K_j|^{-1}\int_{K_j}(G(x,y)\sigma(y)-G(x,z)\sigma(z))\mathrm{d}z\right|^{p_0}\mathrm{d}y\right]^{\frac{2}{p_0}}$$

$$\lesssim |D|^{\frac{2}{p_0}-1}\int_D \left|\sum_{j=1}^n \chi_j(y)|K_j|^{-1}\int_{K_j}(G(x,y)\sigma(y)-G(x,z)\sigma(z))\mathrm{d}z\right|^2\mathrm{d}y$$

$$= |D|^{\frac{2}{p_0}-1}\int_D \sum_{j=1}^n \chi_j(y)|K_j|^{-2}\left|\int_{K_j}(G(x,y)\sigma(y)-G(x,z)\sigma(z))\mathrm{d}z\right|^2\mathrm{d}y$$

$$\lesssim |D|^{\frac{2}{p_0}-1}\sum_{j=1}^n |K_j|^{-1}\int_{K_j}\int_{K_j}|G(x,y)\sigma(y)-G(x,z)\sigma(z)|^2\,\mathrm{d}z\mathrm{d}y,$$

we have

$$\mathbf{E}\left(\int_\Omega\left|\int_D G(x,y)\sigma(y)\mathrm{d}W_y-\int_D G(x,y)\sigma(y)\mathrm{d}W_y^n\right|^2\mathrm{d}x\right)$$

$$\lesssim |D|^{\frac{2}{p_0}-1}\|c\|_{L^{q_0}(B_{2R})}\sum_{j=1}^n |K_j|^{-1}$$

$$\times\int_{K_j}\int_{K_j}\int_\Omega |G(x,y)\sigma(y)-G(x,z)\sigma(z)|^2\mathrm{d}x\mathrm{d}z\mathrm{d}y$$

$$\lesssim \sum_{j=1}^n |K_j|^{-1}\int_{K_j}\int_{K_j}\int_\Omega |G(x,y)\sigma(y)-G(x,z)\sigma(z)|^2\mathrm{d}x\mathrm{d}z\mathrm{d}y.$$

Using the triangle and Cauchy–Schwartz inequalities yields

$$\int_\Omega |G(x,y)\sigma(y)-G(x,z)\sigma(z)|^2\mathrm{d}x$$

$$\lesssim \int_\Omega |G(x,y)-G(x,z)|^2|\sigma(y)|^2\mathrm{d}x+\int_\Omega |G(x,z)|^2|\sigma(y)-\sigma(z)|^2\mathrm{d}x.$$

For $d = 2$, it follows from (2.6), Lemma 2.1, and the η-Hölder continuity of σ that

$$\int_\Omega |G_2(x,y)\sigma(y) - G_2(x,z)\sigma(z)|^2 \mathrm{d}x \lesssim \sigma^2(y)|y-z|^{\frac{3}{2}} + |y-z|^{2\eta},$$

which gives

$$\begin{aligned}
&\mathbf{E}\left(\int_\Omega \left|\int_D G_2(x,y)\sigma(y)\mathrm{d}W_y - \int_D G_2(x,y)\sigma(y)\mathrm{d}W_y^n\right|^2 \mathrm{d}x\right)\\
&\lesssim \sum_{j=1}^n |K_j|^{-1}\int_{K_j}\int_{K_j} \sigma^2(z)|y-z|^{\frac{3}{2}}\mathrm{d}z\mathrm{d}y + \sum_{j=1}^n |K_j|^{-1}\int_{K_j}\int_{K_j} |y-z|^{2\eta}\mathrm{d}z\mathrm{d}y\\
&\le \|\sigma\|^2_{L^2(D)} \max_{1\le j\le n}(\mathrm{diam}K_j)^{\frac{3}{2}} + |D| \max_{1\le j\le n}(\mathrm{diam}K_j)^{2\eta} \to 0
\end{aligned}$$

as $n \to \infty$ since the diameter of $K_j \to 0$ as $n \to \infty$.

For $d = 3$, we have from (2.7), Lemma 2.1, and the η-Hölder continuity of σ that

$$\int_\Omega |G_3(x,y)\sigma(y) - G_3(x,z)\sigma(z)|^2 \mathrm{d}x \lesssim \sigma^2(y)|y-z| + |y-z|^{2\eta},$$

which gives

$$\begin{aligned}
&\mathbf{E}\left(\int_\Omega \left|\int_D G_3(x,y)\sigma(y)\mathrm{d}W_y - \int_D G_3(x,y)\sigma(y)\mathrm{d}W_y^n\right|^2 \mathrm{d}x\right)\\
&\lesssim \sum_{j=1}^n |K_j|^{-1}\int_{K_j}\int_{K_j} \sigma^2(z)|y-z|\mathrm{d}z\mathrm{d}y + \sum_{j=1}^n |K_j|^{-1}\int_{K_j}\int_{K_j} |y-z|^{2\eta}\mathrm{d}z\mathrm{d}y\\
&\lesssim \|\sigma\|^2_{L^2(D)} \max_{1\le j\le n}(\mathrm{diam}K_j) + |D| \max_{1\le j\le n}(\mathrm{diam}K_j)^{2\eta} \to 0
\end{aligned}$$

as $n \to \infty$ since the diameter of $K_j \to 0$ as $n \to \infty$.

For each $n \in \mathbb{N}$, we consider the scattering problem

$$\begin{cases} \Delta u^n + \kappa^2 u^n = g + \sigma \dot{W}_x^n & \text{in } \mathbb{R}^d,\\ \partial_r u^n - \mathrm{i}\kappa u^n = o(r^{-\frac{d-1}{2}}) & \text{as } r \to \infty. \end{cases} \tag{2.11}$$

It follows from $\sigma\dot{W}_x^n \in L^2(D)$ that the problem (2.11) has a unique solution given by

$$u^n(x) = \int_D G(x,y)g(y)\mathrm{d}y + v^n(x). \tag{2.12}$$

Let

$$u(x) = \int_D G(x,y)g(y)\mathrm{d}y + v(x).$$

Since $\mathbf{E}(\|u^n - u\|^2_{L^2(\Omega)}) = \mathbf{E}(\|v^n - v\|^2_{L^2(\Omega)}) \to 0$ as $n \to \infty$, there exists a subsequence of $\{u^n\}$ which converges to u. Letting $n \to \infty$ in (2.12), we obtain the mild solution (2.10) and complete the proof. ∎

Remark 2.8. It is clear to note that the mild solution of the stochastic direct problem (2.10) reduces to the solution of the deterministic direct problem (2.5) when $\sigma = 0$, i.e., no randomness is present in the source.

3. Stochastic inverse problem. In this section, we derive the Fredholm integral equations and develop a regularized Kaczmarz method to solve the stochastic inverse problem by using multifrequency scattering data.

3.1. Integral equations. We assume that the random source is driven by the incoherent white noise so that the variance can be reconstructed. Recall the mild solution at wavenumber κ_j:

$$u(x,\kappa_j) = \int_D G(x,y,\kappa_j)g(y)\mathrm{d}y + \int_D G(x,y,\kappa_j)\sigma(y)\mathrm{d}\widetilde{W}_y. \tag{3.1}$$

Taking the expectation on both sides of (3.1) and using

$$\mathbf{E}\left(\int_D G(x,y,\kappa_j)\sigma(y)\mathrm{d}\widetilde{W}_y\right) = 0,$$

we obtain

$$\mathbf{E}(u(x,\kappa_j)) = \int_D G(x,y,\kappa_j)g(y)\mathrm{d}y,$$

which is a complex-valued Fredholm integral equation of the first kind and may be used to reconstruct g. We point out from the above equation that the reconstruction formula of g looks like the one for the deterministic inverse problem except that the known boundary data is given by the expectation of the radiation wave field. It is more convenient to solve real-valued equations. We split all the complex-valued quantities into their real and imaginary parts.

Let $u = \mathrm{Re}u + \mathrm{iIm}u$ and $G = \mathrm{Re}G + \mathrm{iIm}G$. More explicitly, we have

$$\mathrm{Re}G_2 = \frac{1}{4}Y_0(\kappa_j|x-y|), \quad \mathrm{Im}G_2 = -\frac{1}{4}J_0(\kappa_j|x-y|) \tag{3.2}$$

and

$$\mathrm{Re}G_3 = -\frac{1}{4\pi}\frac{\cos(\kappa_j|x-y|)}{|x-y|}, \quad \mathrm{Im}G_3 = -\frac{1}{4\pi}\frac{\sin(\kappa_j|x-y|)}{|x-y|}. \tag{3.3}$$

Here J_0 and Y_0 are the Bessel function of the first and the second kind with order zero, respectively.

The mild solution (3.1) can be split into real and imaginary parts:

$$\mathrm{Re}u(x,\kappa_j) = \int_D \mathrm{Re}G(x,y,\kappa_j)g(y)\mathrm{d}y + \int_D \mathrm{Re}G(x,y,\kappa_j)\sigma(y)\mathrm{d}\widetilde{W}_y \tag{3.4}$$

and

$$\mathrm{Im}u(x,\kappa_j) = \int_D \mathrm{Im}G(x,y,\kappa_j)g(y)\mathrm{d}y + \int_D \mathrm{Im}G(x,y,\kappa_j)\sigma(y)\mathrm{d}\widetilde{W}_y. \tag{3.5}$$

Noting

$$\mathbf{E}\left(\int_D \mathrm{Re}G(x,y,\kappa_j)\sigma(y)\mathrm{d}\widetilde{W}_y\right) = 0, \quad \mathbf{E}\left(\int_D \mathrm{Im}G(x,y,\kappa_j)\sigma(y)\mathrm{d}\widetilde{W}_y\right) = 0,$$

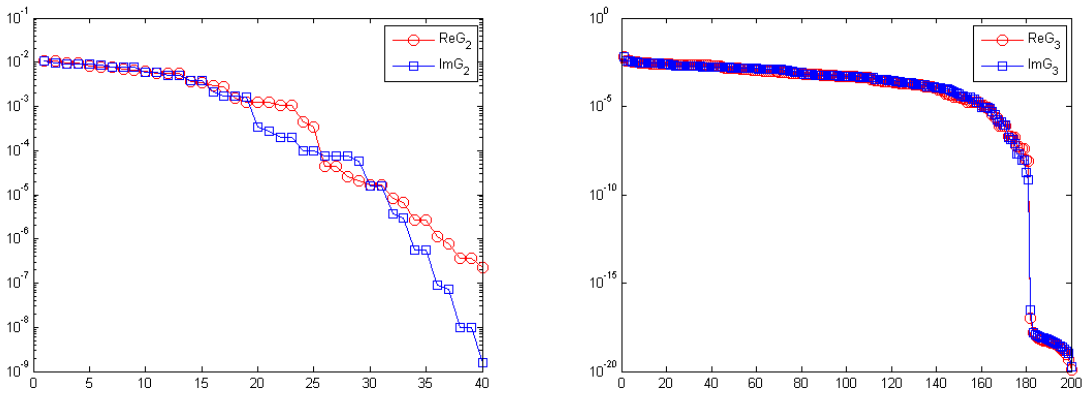

Figure 1. *Log scale for singular values of the Fredholm integral equations for the reconstruction of g: (left) the two-dimensional case; (right) the three-dimensional case.*

we take the expectation on both sides of (3.4) and (3.5) and obtain real-valued Fredholm integral equations of the first kind to reconstruct g:

$$\mathbf{E}(\mathrm{Re}u(x,\kappa_j)) = \int_D \mathrm{Re}G(x,y,\kappa_j)g(y)\mathrm{d}y,$$
$$\mathbf{E}(\mathrm{Im}u(x,\kappa_j)) = \int_D \mathrm{Im}G(x,y,\kappa_j)g(y)\mathrm{d}y.$$

Substituting the real and imaginary parts of the two-dimensional Green function (3.2) and the three-dimensional Green function (3.3) into the above equations yields

$$\mathbf{E}(\mathrm{Re}u(x,\kappa_j)) = \frac{1}{4}\int_D Y_0(\kappa_j|x-y|)g(y)\mathrm{d}y, \tag{3.6}$$

$$\mathbf{E}(\mathrm{Im}u(x,\kappa_j)) = -\frac{1}{4}\int_D J_0(\kappa_j|x-y|)g(y)\mathrm{d}y \tag{3.7}$$

and

$$\mathbf{E}(\mathrm{Re}u(x,\kappa_j)) = -\frac{1}{4\pi}\int_D \frac{\cos(\kappa_j|x-y|)}{|x-y|}g(y)\mathrm{d}y, \tag{3.8}$$

$$\mathbf{E}(\mathrm{Im}u(x,\kappa_j)) = -\frac{1}{4\pi}\int_D \frac{\sin(\kappa_j|x-y|)}{|x-y|}g(y)\mathrm{d}y. \tag{3.9}$$

It is known that Fredholm integral equations of the first kind are ill-posed due to rapidly decaying singular values of matrices from the discretized integral kernels. Appropriate regularization methods are needed to recover the information about the solutions as stably as possible. As a representative example, Figure 1 plots the singular values of the matrices for the Fredholm integral equations (3.6)–(3.9) at $\kappa = 2.5\pi$, where in the y-axis we use a base 10 logarithmic scale. We can observe similar decaying patterns of the singular values for (3.6), (3.7) for the two-dimensional case and (3.8), (3.9) for the three-dimensional case. It will not

make much difference to use (3.6) or (3.7) to reconstruct g in two dimensions or to use (3.8) or (3.9) to reconstruct g in three dimensions.

Using the identities in Proposition A.2,

$$\mathbf{E}\left(\left|\int_D \mathrm{Re}G(x,y,\kappa_j)\sigma(y)\mathrm{d}\widetilde{W}_y\right|^2\right) = \int_D |\mathrm{Re}G(x,y,\kappa_j)|^2\sigma^2(y)\mathrm{d}y$$

and

$$\mathbf{E}\left(\left|\int_D \mathrm{Im}G(x,y,\kappa_j)\sigma(y)\mathrm{d}\widetilde{W}_y\right|^2\right) = \int_D |\mathrm{Im}G(x,y,\kappa_j)|^2\sigma^2(y)\mathrm{d}y,$$

we take the variance on both sides of (3.4) and (3.5) and obtain

$$\mathbf{V}(\mathrm{Re}u(x,\kappa_j)) = \int_D |\mathrm{Re}G(x,y,\kappa_j)|^2\sigma^2(y)\mathrm{d}y,$$
$$\mathbf{V}(\mathrm{Im}u(x,\kappa_j)) = \int_D |\mathrm{Im}G(x,y,\kappa_j)|^2\sigma^2(y)\mathrm{d}y,$$

which are the Fredholm integral equations of the first kind to reconstruct the variance. Again, we substitute (3.2) and (3.3) into the above equations and get

$$\mathbf{V}(\mathrm{Re}u(x,\kappa_j)) = \frac{1}{16}\int_D Y_0^2(\kappa_j|x-y|)\sigma^2(y)\mathrm{d}y, \tag{3.10}$$

$$\mathbf{V}(\mathrm{Im}u(x,\kappa_j)) = \frac{1}{16}\int_D J_0^2(\kappa_j|x-y|)\sigma^2(y)\mathrm{d}y \tag{3.11}$$

and

$$\mathbf{V}(\mathrm{Re}u(x,\kappa_j)) = \frac{1}{16\pi^2}\int_D \frac{\cos^2(\kappa_j|x-y|)}{|x-y|^2}\sigma^2(y)\mathrm{d}y, \tag{3.12}$$

$$\mathbf{V}(\mathrm{Im}u(x,\kappa_j)) = \frac{1}{16\pi^2}\int_D \frac{\sin^2(\kappa_j|x-y|)}{|x-y|^2}\sigma^2(y)\mathrm{d}y. \tag{3.13}$$

To investigate ill-posedeness of the above four equations, we plot their singular values in Figure 2. It can be seen that (3.10), (3.11) and (3.12), (3.13) show almost identical distributions of the singular values for the two- and three-dimensional cases, respectively. The singular values decay exponentially to zeros and there is a big gap between the few leading singular values and the rests. Hence it is severely ill-posed to use directly either (3.10) or (3.11) and (3.12) or (3.13) to reconstruct σ^2. Subtracting (3.11) from (3.10) and (3.13) from (3.12), we obtain improved equations to reconstruct σ^2 in both two- and three-dimensional cases:

$$\mathbf{V}(\mathrm{Re}u(x,\kappa_j)) - \mathbf{V}(\mathrm{Im}u(x,\kappa_j)) = \frac{1}{16}\int_D \left(Y_0^2(\kappa_j|x-y|) - J_0^2(\kappa_j|x-y|)\right)\sigma^2(y)\mathrm{d}y, \tag{3.14}$$

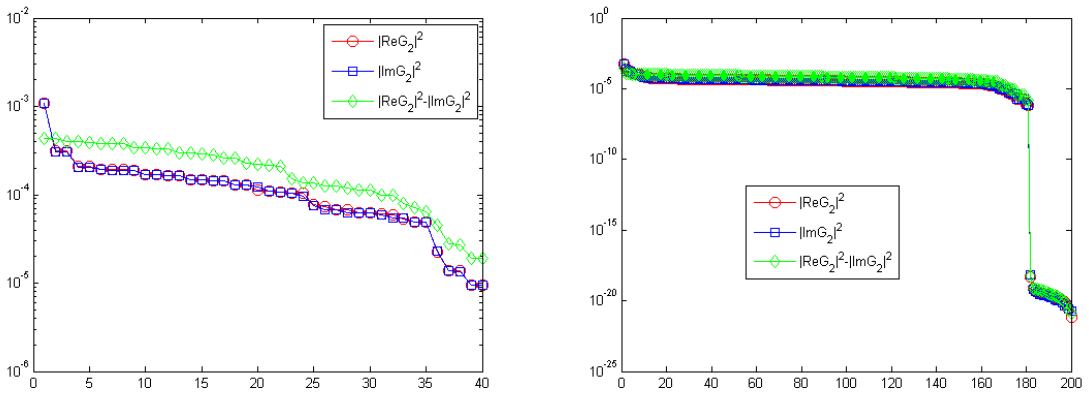

Figure 2. *Log scale for singular values of the Fredholm integral equations for the reconstruction of σ^2: (left) the two-dimensional case; (right) the three-dimensional case.*

$$\mathbf{V}(\mathrm{Re}u(x,\kappa_j)) - \mathbf{V}(\mathrm{Im}u(x,\kappa_j)) = \frac{1}{16\pi^2}\int_D \frac{\cos(2\kappa_j|x-y|)}{|x-y|^2}\sigma^2(y)\mathrm{d}y. \tag{3.15}$$

In fact, it is clear to note in Figure 2 that the singular values of (3.14) and (3.15) display better behavior that those of (3.10), (3.11) and (3.12), (3.13). They decay more slowly and distribute more uniformly. Numerically, (3.14) and (3.15) do give much better reconstructions. We will only show the results by using (3.14) and (3.15) in the numerical experiments.

Mathematically, the reconstruction formulas require the knowledge of the expectation of the real data. Based on the strong law of large numbers, the expected value of a random variable can be approximated by the average obtained from a large number of trials. The average will tend to become closer to the expectation as more trials are performed. Since we can only take finitely many trials, the actual input will always contain noise.

3.2. Numerical method. In this section, we propose a regularized Kaczmarz method to solve the ill-posed integral equations. The classical Kaczmarz algorithm is an iterative method for solving linear systems of algebraic equations [29]. The idea is to project the current approximation solution successively onto each of the hyperplanes. It turns out that such a procedure converges to the minimum norm solution of the system provided that the solution set is nonempty.

Consider the following operator equations:

$$A_j q = p_j, \quad j = 1, \ldots, m, \tag{3.16}$$

where the index j means different wavenumber κ_j, q represents the unknown g or σ^2, and p_j is the given data. We take (3.6) as an example, q is the unknown g, p_j denotes the boundary data $\mathbf{E}(\mathrm{Re}u(x,\kappa_j))$, and the operator A_j is given by

$$A_j q(x) = \frac{1}{4}\int_D Y_0(\kappa_j|x-y|)q(y)dy.$$

Letting the initial guess $q^0 = 0$, the classical Kaczmarz method for solving (3.16) reads as follows: For $k = 0, 1, \ldots,$

$$\begin{cases} q_0 = q^k, \\ q_j = q_{j-1} + A_j^*(A_j A_j^*)^{-1}(p_j - A_j q_{j-1}), \quad j = 1, \ldots, m, \\ q^{k+1} = q_m, \end{cases} \tag{3.17}$$

where A_j^* is the adjoint operator of A_j. In (3.17), there are two loops: the outer loop is carried for iterative index k and the inner loop is done for the different wavenumber κ_j. In practice, the operator $A_j A_j^*$ may not be invertible or is ill-conditioned even if it is invertible. A regularization technique is needed.

We propose a regularized Kaczmarz method: Let the initial guess $q^0 = 0$,

$$\begin{cases} q_0 = q^k, \\ q_j = q_{j-1} + A_j^*(\mu I + A_j A_j^*)^{-1}(p_j - A_j q_{j-1}), \quad j = 1, \ldots, m, \\ q^{k+1} = q_m, \end{cases} \tag{3.18}$$

for $k = 0, 1, \ldots,$ where $\mu > 0$ is the regularization parameter and I is the identity operator. Although there are two loops in (3.18), the operator $\mu I + A_j A_j^*$ leads to small scale linear system of equations with size equal to the number of measurements. Moreover, they essentially need to be solved only m times by a direct solver such as the LU decomposition since A_j keep unchanged in the outer loop.

4. Numerical experiments.

In this section, we discuss the algorithmic implementation for the direct and inverse random source scattering problems and present one two-dimensional example and one three-dimensional example to demonstrate the validity and effectiveness of the proposed method.

The scattering data is obtained by the numerical solution of the stochastic Helmholtz equation instead of the numerical integration of the Fredholm integral equations in order to avoid the so-called inverse crime. Although the stochastic Helmholtz equation can be more efficiently solved by using the Wiener chaos expansions to obtain statistical moments such as the mean and variance [5], we choose the Monte Carlo method to simulate the actual process of measuring data. In each realization, the stochastic Helmholtz equation is solved by using the finite element method with the perfectly matched layer (PML) technique [13]. After all the realizations are done, we take an average of the solutions and use it as approximated scattering data to either the mean or the variance. It is clear to note that the data is more accurate as more realizations are taken. In the following two examples, we take five equally spaced wavenumbers $\kappa_j = (j+0.5)\pi, j = 0, \ldots, 4$; the regularization parameter μ is 1.0×10^{-7}; the number of the outer loop for the Kaczmarz iteration is 5; the total number of realizations is 10^5.

First we consider a two-dimensional example. Let

$$g(x_1, x_2) = 0.3(1 - x_1)^2 e^{-x_1^2 - (x_2+1)^2} - (0.2x_1 - x_1^3 - x_2^5)e^{-x_1^2 - x_2^2} - 0.03e^{-(x_1+1)^2 - x_2^2}$$

and

$$\sigma(x_1, x_2) = 0.6e^{-8(r^3 - 0.75r^2)}, \quad r = (x_1^2 + x_2^2)^{1/2},$$

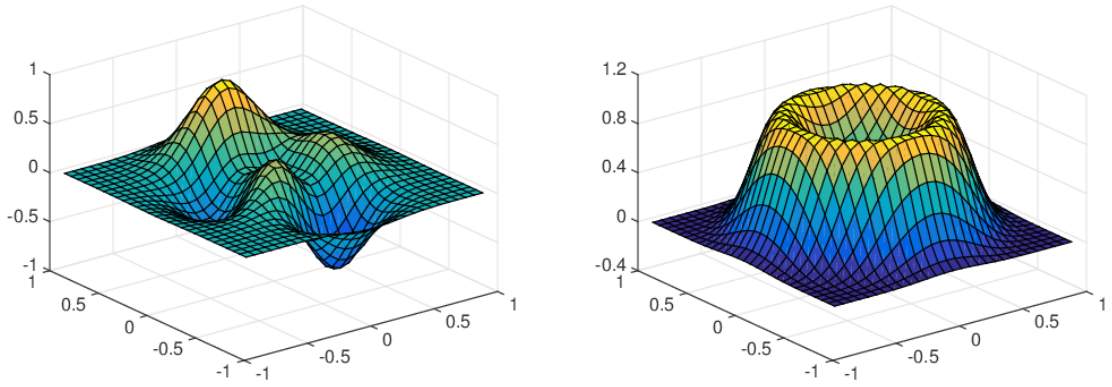

Figure 3. *The two-dimensional example: (left) surface plot of the exact mean g_1; (right) surface plot of the exact variance σ_1.*

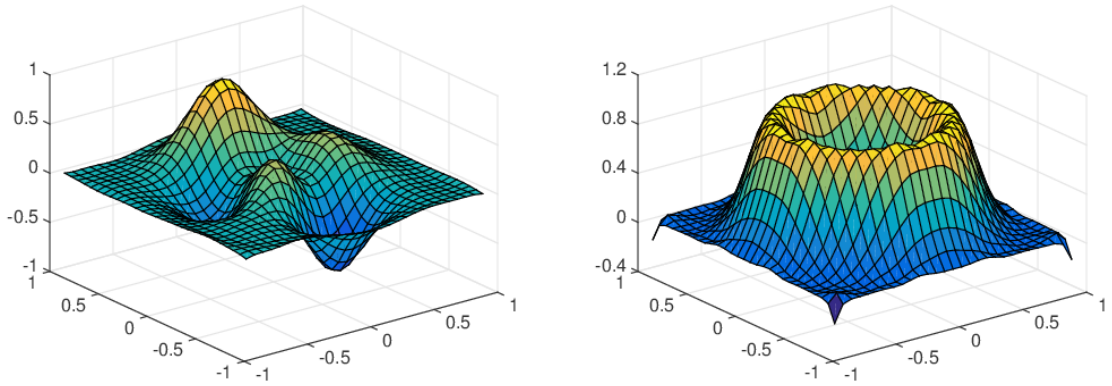

Figure 4. *Two-dimensional example: (left) surface plot of the reconstructed mean g_1; (right) surface plot of the reconstructed variance σ_1.*

and reconstruct the mean g_1 and the variance σ_1 given by

$$g_1(x_1, x_2) = g(3x_1, 3x_2) \quad \text{and} \quad \sigma_1(x_1, x_2) = \sigma^2(x_1, x_2)$$

inside the domain $D_1 = [-1, 1] \times [-1, 1]$. See Figure 3 for the surface plot of the exact g_1 (left) and σ_1 (right). The computational domain is set to be $[-3, 3] \times [-3, 3]$ with the PML thickness 0.5. After the direct problem is solved and the value of u is obtained at the grid points, the linear interpolation is used to generate the synthetic data at 40 uniformly distributed points on the circle with radius 2, i.e., $x_1 = 2\cos\theta_i, x_2 = 2\sin\theta_i, \theta_i = i\pi/20, i = 0, 1, \ldots, 39$. Figure 4 shows the reconstructed mean g_1 and variance σ_1.

Next we consider a three-dimensional example. Denote $D_2 = [-1, 1] \times [-1, 1] \times [-1, 1]$. Let

$$g(x_1, x_2, x_3) = \sin(\pi x_1)\sin(\pi x_2)\sin(\pi x_3)$$

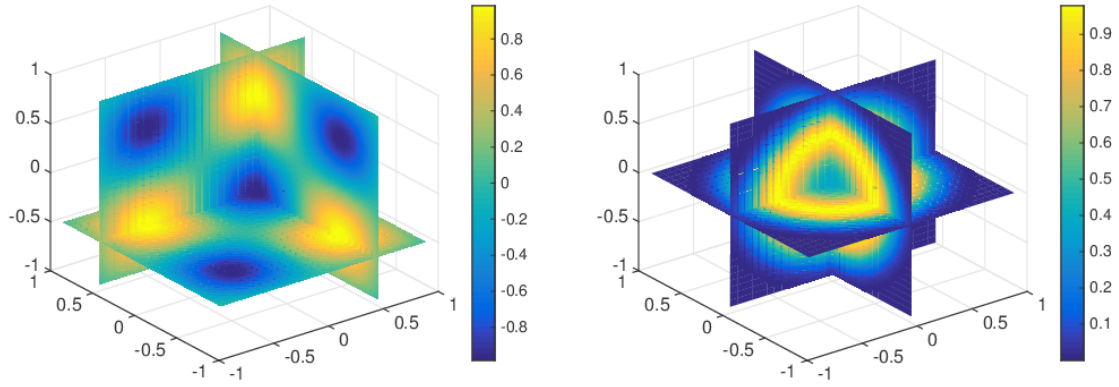

Figure 5. *Three-dimensional example: (left) cross-section plot of the exact mean g_2 at $x_1 = 0.5, x_2 = 0.5, x_3 = -0.5$; (right) cross-section plot of the exact variance σ_2 at $x_1 = 0.0, x_2 = 0.0, x_3 = 0.0$.*

and

$$\sigma(x_1, x_2, x_3) = 0.6e^{-8(r^3 - 0.75r^2)}, \quad r = (x_1^2 + x_2^2 + x_3^2)^{1/2},$$

and reconstruct the mean g_2 and the variance σ_2 given by

$$g_2(x_1, x_2, x_3) = \begin{cases} g(x_1, x_2, x_3), & x \in D_2, \\ 0, & x \notin D_2, \end{cases}$$

and

$$\sigma_2(x_1, x_2, x_3) = \sigma^2(x_1, x_2, x_3),$$

inside the domain D_2. See Figure 5 for the cross-section plots of the exact g_2 (left) at $x_1 = 0.5, x_2 = 0.5, x_3 = -0.5$, and σ_2 (right) at $x_1 = 0.0, x_2 = 0.0, x_3 = 0.0$. The computational domain is set to be $[-3, 3] \times [-3, 3] \times [-3, 3]$ with the PML thickness 0.5. After the direct problem is solved and the value of u is obtained at the grid points, the linear interpolation is used to generate the synthetic data on the sphere with radius 2 and equally spaced 10×20 points in the (θ, φ) plane, i.e, $x_1 = 2\sin\theta_i \cos\varphi_j, x_2 = 2\sin\theta_i \sin\varphi_j, x_3 = 2\cos\theta_i, \theta_i = i\pi/10, \varphi_j = j\pi/10, i = 0, 1, \ldots, 9, j = 0, 1, \ldots, 19$. Figure 6 shows the reconstructed mean g_2 and variance σ_2.

5. Conclusion. We have studied an inverse random source scattering problem for the two- and three-dimensional Helmholtz equation where the source is driven by an additive white noise or colored noise. Under a suitable regularity assumption of the source functions g and σ, the direct scattering problem is shown constructively to have a unique mild solution which is given explicitly as an integral equation. Based on the explicit solution, Fredholm integral equations are deduced for the inverse scattering problem to reconstruct the mean and the variance of the random source. We propose the regularized Kaczmarz method to solve the ill-posed integral equations by using multiple frequency data. Numerical examples, one

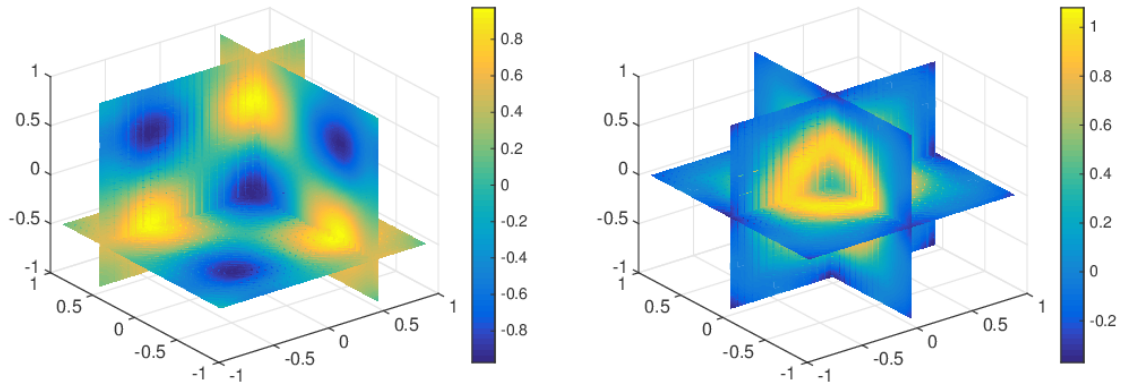

Figure 6. *Three-dimensional example: (left) cross-section plot of the reconstructed mean g_2 at $x_1 = 0.5, x_2 = 0.5, x_3 = -0.5$; (right) cross-section plot of the reconstructed variance σ_2 at $x_1 = 0.0, x_2 = 0.0$, $x_3 = 0.0$.*

two-dimensional example and one three-dimensional example, are presented to demonstrate the validity and effectiveness of the proposed method. We are currently investigating the inverse random source scattering problem in an inhomogeneous medium where the explicit Green function is no longer available. Although this paper concerns the inverse random source scattering problem for the Helmholtz equation, we believe that the proposed framework and methodology can be directly applied to solve many other inverse random source problems and even more general stochastic inverse problems. For instance, it is interesting to study inverse random source problems for the stochastic Poisson, heat, and wave equations. It is interesting and challenging to consider the inverse random medium scattering problem where the medium should be modeled as a random function. We hope to be able to report the progress on these problems in the future.

Appendix A. White noise.

Let us first introduce the d-parameter Brownian sheet, which is also called d-parameter Brownian motion, on $(\mathbb{R}^d_+, \mathcal{B}(\mathbb{R}^d_+), \mu)$, where $d \in \mathbb{N}, \mathbb{R}^d_+ = \{x = (x_1, \ldots, x_d) \in \mathbb{R}^d : x_j \geq 0, j = 1, \ldots, d\}$, $\mathcal{B}(\mathbb{R}^d_+)$ is the Borel σ-algebra of $\mathbb{R}^d_+$, and μ is the Lebesgue measure. If $x \in \mathbb{R}^d_+$, let $(0, x] = (0, x_1] \times \cdots \times (0, x_d]$.

Definition A.1. *The Brownian sheet on $\mathbb{R}^d_+$ is the process $\{\widetilde{W}_x : x \in \mathbb{R}^d_+\}$ defined by $\widetilde{W}_x = \widetilde{W}\{(0, x]\}$, where $\widetilde{W}$ is a random set function satisfying*

1. *$\forall A \in \mathcal{B}(\mathbb{R}^d_+)$, $\widetilde{W}(A)$ is a $\mathcal{N}(0, \mu(A))$ random variable;*
2. *$\forall A, B \in \mathcal{B}(\mathbb{R}^d_+)$, if $A \cap B = \emptyset$, then $\widetilde{W}(A)$ and $\widetilde{W}(B)$ are independent and $\widetilde{W}(A \cup B) = \widetilde{W}(A) + \widetilde{W}(B)$.*

It can be verified from Definition A.1 that

$$\mathbf{E}(\widetilde{W}(A)\widetilde{W}(B)) = \mu(A \cap B) \quad \forall\ A, B \in \mathcal{B}(\mathbb{R}^d_+),$$

which gives the covariance function of the Brownian sheet

$$\mathbf{E}(\widetilde{W}_x \widetilde{W}_y) = x \wedge y := (x_1 \wedge y_1) \cdots (x_d \wedge y_d) \tag{A.1}$$

for any $x = (x_1, \ldots, x_d) \in \mathbb{R}^d_+$ and $y = (y_1, \ldots, y_d) \in \mathbb{R}^d_+$, where $x_j \wedge y_j = \min\{x_j, y_j\}$.

The Brownian sheet can be generalized to be defined on the whole space $\mathbb{R}^d$ by introducing 2^d independent Brownian sheets defined on $\mathbb{R}^d_+$. Define a multi-index $t = (t_1, \ldots, t_d)$ with $t_j = \{1, -1\}$ for $j = 1, \ldots, d$. Introduce 2^d independent Brownian sheets $\{\widetilde{W}^t\}$ defined on $\mathbb{R}^d_+$. For any $x = (x_1, \ldots, x_d) \in \mathbb{R}^d$, define the Brownian sheet

$$\widetilde{W}_x := \widetilde{W}^{t(x)}_{\breve{x}},$$

where $\breve{x} = (|x_1|, \ldots, |x_d|)$ and $t(x) = (\mathrm{sgn}(x_1), \ldots, \mathrm{sgn}(x_d))$. The sign function $\mathrm{sgn}(x_j) = 1$ if $x_j \geq 0$, otherwise $\mathrm{sgn}(x_j) = -1$.

In two or more parameters, white noise can be thought of as the derivative of the Brownian sheet. In fact, the Brownian sheet $\widetilde{W}_x$ is nowhere-differentiable in the ordinary sense, but its derivatives will exist in the sense of Schwartz distributions. Define

$$\dot{\widetilde{W}}_x = \frac{\partial^d \widetilde{W}_x}{\partial x_1 \cdots \partial x_d}.$$

If $\phi(x)$ is a deterministic square-integrable complex-valued test function with a compact support in $\mathbb{R}^d$, then $\dot{\widetilde{W}}_x$ is the distribution

$$\dot{\widetilde{W}}_x(\phi) = (-1)^n \int_{\mathbb{R}^n} \widetilde{W}_x \frac{\partial^n \phi(x)}{\partial x_1 \cdots \partial x_n} \mathrm{d}x.$$

We may define the stochastic integral

$$\int_{\mathbb{R}^n} \phi(x) \mathrm{d}\widetilde{W}_x = (-1)^d \int_{\mathbb{R}^d} \widetilde{W}_x \frac{\partial^d \phi(x)}{\partial x_1 \cdots \partial x_d} \mathrm{d}x. \tag{A.2}$$

Proposition A.2. *Let $\phi(x)$ be a test function with a compact support in $\mathbb{R}^d$. It holds that*

$$\mathbf{E}\left(\int_{\mathbb{R}^d} \phi(x) \mathrm{d}\widetilde{W}_x\right) = 0, \quad \mathbf{E}\left(\left|\int_{\mathbb{R}^d} \phi(x) \mathrm{d}\widetilde{W}_x\right|^2\right) = \int_{\mathbb{R}^n} |\phi(x)|^2 \mathrm{d}x.$$

Proof. It follows from (A.2) that

$$\mathbf{E}\left(\int_{\mathbb{R}^d} \phi(x) \mathrm{d}\widetilde{W}_x\right) = (-1)^d \int_{\mathbb{R}^d} \frac{\partial^d \phi(x)}{\partial x_1 \cdots \partial x_d} \mathbf{E}(\widetilde{W}_x) \mathrm{d}x = 0.$$

Using (A.1), we have

$$\begin{aligned}
\mathbf{E}\left(\left|\int_{\mathbb{R}^d} \phi(x) \mathrm{d}\widetilde{W}_x\right|^2\right) &= \mathbf{E}\left(\int_{\mathbb{R}^d} \widetilde{W}_x \frac{\partial^d \phi(x)}{\partial x_1 \cdots \partial x_d} \mathrm{d}x \times \int_{\mathbb{R}^d} \widetilde{W}_y \frac{\partial^d \bar{\phi}(y)}{\partial y_1 \cdots \partial y_d} \mathrm{d}y\right) \\
&= \int_{\mathbb{R}^d} \int_{\mathbb{R}^d} \frac{\partial^d \phi(x)}{\partial x_1 \cdots \partial x_d} \frac{\partial^d \bar{\phi}(y)}{\partial y_1 \cdots \partial y_d} \mathbf{E}(\widetilde{W}_x \widetilde{W}_y) \mathrm{d}x \mathrm{d}y \\
&= \int_{\mathbb{R}^d} \frac{\partial^d \bar{\phi}(y)}{\partial y_1 \cdots \partial y_d} \left(\int_{\mathbb{R}^d} \frac{\partial^d \phi(x)}{\partial x_1 \cdots \partial x_d} (x \wedge y) \mathrm{d}x\right) \mathrm{d}y.
\end{aligned}$$

We claim that

$$\int_{\mathbb{R}^d} \frac{\partial^d \phi(x)}{\partial x_1 \cdots \partial x_d}(x \wedge y)\mathrm{d}x = (-1)^d \int_{-\infty}^{y_1} \cdots \int_{-\infty}^{y_d} \phi(x)\mathrm{d}x_d \cdots \mathrm{d}x_1, \tag{A.3}$$

which is proved in the following by the method of induction.

First, we show (A.3) for $d = 1$. Using the integration by parts yields

$$\begin{aligned}\int_{\mathbb{R}} \frac{\partial \phi(x_1)}{\partial x_1}(x_1 \wedge y_1)\mathrm{d}x_1 &= \int_{-\infty}^{y_1} \frac{\partial \phi(x_1)}{\partial x_1} x_1 \mathrm{d}x_1 + \int_{y_1}^{\infty} \frac{\partial \phi(x_1)}{\partial x_1} y_1 \mathrm{d}x_1 \\ &= x_1\phi(x_1)\big|_{-\infty}^{y_1} - \int_{-\infty}^{y_1} \phi(x_1)\mathrm{d}x_1 + y_1\phi(x_1)\big|_{y_1}^{\infty} = -\int_{-\infty}^{y_1} \phi(x_1)\mathrm{d}x_1.\end{aligned}$$

We assume that (A.3) is valid for a $d \in \mathbb{N}$, i.e.,

$$\int_{\mathbb{R}^d} \frac{\partial^d \phi(x)}{\partial x_1 \cdots \partial x_d}(x \wedge y)\mathrm{d}x = (-1)^d \int_{-\infty}^{y_1} \cdots \int_{-\infty}^{y_d} \phi(x)\mathrm{d}x_d \cdots \mathrm{d}x_1.$$

Next we show that (A.3) holds for $d+1$. Let $x = (x_1, \ldots, x_d) \in \mathbb{R}^d, y = (y_1, \ldots, y_d) \in \mathbb{R}^d$, and $x_{d+1}, y_{d+1} \in \mathbb{R}$. Denote $\partial x = \partial x_1 \cdots \partial x_d$. It follows from the integration by parts that

$$\begin{aligned}&\int_{\mathbb{R}^{d+1}} \frac{\partial^{d+1}\phi(x, x_{d+1})}{\partial x \partial x_{d+1}}(x \wedge y)(x_{d+1} \wedge y_{d+1})\mathrm{d}x\mathrm{d}x_{d+1} \\ &= \int_{\mathbb{R}^d} \int_{-\infty}^{y_{d+1}} \frac{\partial}{\partial x_{d+1}} \left(\frac{\partial^d \phi(x, x_{d+1})}{\partial x} \right) (x \wedge y) x_{d+1} \mathrm{d}x_{d+1}\mathrm{d}x \\ &\quad + \int_{\mathbb{R}^d} \int_{y_{d+1}}^{\infty} \frac{\partial}{\partial x_{d+1}} \left(\frac{\partial^d \phi(x, x_{d+1})}{\partial x} \right) (x \wedge y) y_{d+1} \mathrm{d}y_{d+1}\mathrm{d}x \\ &= y_{d+1} \int_{\mathbb{R}^d} \frac{\partial^d \phi(x, y_{d+1})}{\partial x}(x \wedge y)\mathrm{d}x - \int_{\mathbb{R}^d} \int_{-\infty}^{y_{d+1}} \frac{\partial^d \phi(x, x_{d+1})}{\partial x}(x \wedge y)\mathrm{d}x_{d+1}\mathrm{d}x \\ &\quad - y_{d+1} \int_{\mathbb{R}^d} \frac{\partial^d \phi(x, y_{d+1})}{\partial x}(x \wedge y)\mathrm{d}x \\ &= (-1)^{d+1} \int_{-\infty}^{y_1} \cdots \int_{-\infty}^{y_d} \int_{-\infty}^{y_{d+1}} \phi(x, x_{d+1})\mathrm{d}x_{d+1}\mathrm{d}x,\end{aligned}$$

which completes the proof of (A.3).

Combining the above estimates, we obtain

$$\begin{aligned}\mathbf{E}\left(\left| \int_{\mathbb{R}^d} \phi(x)\mathrm{d}\widetilde{W}_x \right|^2 \right) &= \int_{\mathbb{R}^d} \frac{\partial^d \bar{\phi}(y)}{\partial y_1 \ldots \partial y_d} \left(\int_{-\infty}^{y_1} \cdots \int_{-\infty}^{y_d} \phi(x)\mathrm{d}x \right) \mathrm{d}y \\ &= \int_{\mathbb{R}^d} |\phi(x)|^2 \mathrm{d}x,\end{aligned}$$

which completes the proof. ∎

Appendix B. Colored noise. Let Q be a nonnegative and symmetric trace class linear operator which can be described by a kernel $k(x, y)$:

$$(Qf)(x) = \int_{\mathbb{R}^d} k(x, y) f(y) \mathrm{d}y, \quad x, y \in \mathbb{R}^d.$$

A colored noise, as the formal derivative of a stochastic process W_x, denoted by $\dot{W}(x)$, can be defined via the following approach:

$$\dot{W}_x = Q\dot{\widetilde{W}}_x,$$

where $\dot{\widetilde{W}}_x$ is the white noise. If the linear operator Q commutes with the differential operator $\partial^d/\partial x_1 \cdots \partial x_d$, then the stochastic process $W_x = Q\widetilde{W}_x$ with $\widetilde{W}_x$ being the standard d-parameter Brownian motion.

For any $A, B \in \mathcal{B}(\mathbb{R}^d)$, $W(A)$ satisfies

$$W(A) \sim \mathcal{N}\left(0, \int_A \int_A c(x, y) \mathrm{d}x \mathrm{d}y\right)$$

and

$$\mathbf{E}(W(A)W(B)) = \int_A \int_B c(x, y) \mathrm{d}x \mathrm{d}y,$$

where c is the correlation function of $\dot{W}(x)$ and is given by

$$\begin{aligned} c(x, y) :&= \mathbf{E}\left(\dot{W}_x \dot{W}_y\right) = \mathbf{E}\left(\int_{\mathbb{R}^d} k(x, z) \mathrm{d}\widetilde{W}_z \times \int_{\mathbb{R}^d} k(y, z) \mathrm{d}\widetilde{W}_z\right) \\ &= \int_{\mathbb{R}^d} k(x, z) k(y, z) \mathrm{d}z. \end{aligned}$$

Specially, if $c(x, y) = \delta(x - y)$, i.e., Q is the identity operator, then the colored noise reduces the white noise.

If $\phi(x)$ is a deterministic square-integrable complex-valued test function with a compact support in $\mathbb{R}^d$, then $\dot{W}_x$ is also the distribution

$$\dot{W}_x(\phi) = (-1)^d \int_{\mathbb{R}^d} W_x \frac{\partial^d \phi(x)}{\partial x_1 \cdots \partial x_d} \mathrm{d}x,$$

which is equivalent to

$$\dot{W}_x(\phi) = \dot{\widetilde{W}}_x(Q\phi) = (-1)^d \int_{\mathbb{R}^d} \widetilde{W}_x \frac{\partial^d (Q\phi)(x)}{\partial x_1 \cdots \partial x_d} \mathrm{d}x.$$

We may define a stochastic integral with respect to the colored noise by

$$\int_{\mathbb{R}^d} \phi(x) \mathrm{d}W_x = (-1)^d \int_{\mathbb{R}^d} W_x \frac{\partial^d \phi(x)}{\partial x_1 \cdots \partial x_d} \mathrm{d}x$$

or equivalently

$$\int_{\mathbb{R}^d} \phi(x) \mathrm{d}W_x = (-1)^d \int_{\mathbb{R}^d} \widetilde{W}_x \frac{\partial^d (Q\phi)(x)}{\partial x_1 \cdots \partial x_d} \mathrm{d}x. \tag{B.1}$$

Proposition B.1. *Let $\phi(x)$ be a test function with a compact support in $\mathbb{R}^d$. It holds that*

$$\mathbf{E}\left(\int_{\mathbb{R}^d}\phi(x)\mathrm{d}W_x\right)=0,\quad \mathbf{E}\left(\left|\int_{\mathbb{R}^d}\phi(x)\mathrm{d}W_x\right|^2\right)=\int_{\mathbb{R}^d}\int_{\mathbb{R}^d}\phi(x)c(x,y)\bar{\phi}(y)\mathrm{d}x\mathrm{d}y.$$

Proof. Using (B.1), we get

$$\mathbf{E}\left(\int_{\mathbb{R}^d}\phi(x)\mathrm{d}W_x\right)=(-1)^d\int_{\mathbb{R}^d}\frac{\partial^d(Q\phi)(x)}{\partial x_1\cdots\partial x_d}\mathbf{E}(\widetilde{W}_x)\mathrm{d}x=0.$$

It follows from (A.1) and (B.1) that

$$\begin{aligned}\mathbf{E}\left(\left|\int_{\mathbb{R}^d}\phi(x)\mathrm{d}W_x\right|^2\right)&=\mathbf{E}\left(\int_{\mathbb{R}^d}\widetilde{W}_x\frac{\partial^d(Q\phi)(x)}{\partial x_1\cdots\partial x_d}\mathrm{d}x\times\int_{\mathbb{R}^d}\widetilde{W}_y\frac{\partial^d(Q\bar{\phi})(y)}{\partial y_1\cdots\partial y_d}\mathrm{d}y\right)\\&=\int_{\mathbb{R}^d}\int_{\mathbb{R}^d}\frac{\partial^d(Q\phi)(x)}{\partial x_1\cdots\partial x_d}\frac{\partial^d(Q\bar{\phi})(y)}{\partial y_1\cdots\partial y_d}\mathbf{E}(\widetilde{W}_x\widetilde{W}_y)\mathrm{d}x\mathrm{d}y\\&=\int_{\mathbb{R}^d}\int_{\mathbb{R}^d}\frac{\partial^d(Q\phi)(x)}{\partial x_1\cdots\partial x_d}\frac{\partial^d(Q\bar{\phi})(y)}{\partial y_1\cdots\partial y_d}(x\wedge y)\mathrm{d}x\mathrm{d}y.\end{aligned}$$

Following the same proof for Proposition A.2, we have

$$\begin{aligned}\mathbf{E}\left(\left|\int_{\mathbb{R}^d}\phi(x)\mathrm{d}W_x\right|^2\right)&=\int_{\mathbb{R}^d}(Q\phi)(x)(Q\bar{\phi})(x)\mathrm{d}x\\&=\int_{\mathbb{R}^d}\left(\int_{\mathbb{R}^d}k(x,y)\phi(y)\mathrm{d}y\right)\left(\int_{\mathbb{R}^d}k(x,z)\bar{\phi}(z)\mathrm{d}z\right)\mathrm{d}x\\&=\int_{\mathbb{R}^d}\int_{\mathbb{R}^d}\phi(y)\bar{\phi}(z)\left(\int_{\mathbb{R}^d}k(x,y)k(x,z)\mathrm{d}x\right)\mathrm{d}y\mathrm{d}z\\&=\int_{\mathbb{R}^d}\int_{\mathbb{R}^d}\phi(y)\bar{\phi}(z)c(y,z)\mathrm{d}y\mathrm{d}z,\end{aligned}$$

which completes the proof. ∎

REFERENCES

[1] R. Adams and J. Fournier, *Sobolev Spaces*, 2nd ed., Academic Press, Amsterdam, 2003.

[2] R. Albanese and P. Monk, *The inverse source problem for Maxwell's equations*, Inverse Problems, 22 (2006), pp. 1023–1035.

[3] H. Ammari, G. Bao, and J. Fleming, *An inverse source problem for Maxwell's equations in magnetoencephalography*, SIAM J. Appl. Math., 62 (2002), pp. 1369–1382.

[4] A. Badia and T. Nara, *An inverse source problem for Helmholtz's equation from the Cauchy data with a single wave number*, Inverse Problems, 27 (2011), 105001.

[5] M. Badieirostami, A. Adibi, H.-M. Zhou, and S.-N. Chow, *Wiener chaos expansion and simulation of electromagnetic wave propagation excited by a spatially incoherent source*, Multiscale Model. Simul., 8 (2010), pp. 591–604.

[6] G. Bao, S.-N. Chow, P. Li, and H.-M. Zhou, *An inverse random source problem for the Helmholtz equation*, Math. Comp., 83 (2014), pp. 215–233.

[7] G. Bao, P. Li, J. Lin, and F. Triki, *Inverse scattering problems with multi-frequencies*, Inverse Problems, 31 (2015), 093001.
[8] G. Bao, J. Lin, and F. Triki, *A multi-frequency inverse source problem*, J. Differential Equations, 249 (2010), pp. 3443–3465.
[9] G. Bao, S. Lu, W. Rundell, and B. Xu, *A recursive algorithm for multifrequency acoustic inverse source problems*, SIAM J. Numer. Anal., 53 (2015), pp. 1608–1628.
[10] G. Bao and X. Xu, *An inverse random source problem in quantifying the elastic modulus of nanomaterials*, Inverse Problems, 29 (2013), 015006.
[11] A. Calderón, *On an inverse boundary value problem*, in Proceedings of the Seminar on Numerical Analysis and Its Applications to Continuum Physics, Rio de Janeiro, 1980, pp. 65–73.
[12] Y.-Z. Cao, R. Zhang, and K. Zhang, *Finite element method and discontinuous Galerkin method for stochastic Helmholtz equation in two- and three-dimensions*, J. Comput. Math., 26 (2008), pp. 701–715.
[13] Z. Chen and X. Liu, *An adaptive perfectly matched layer technique for time-harmonic scattering problems*, SIAM J. Numer. Anal., 43 (2005), pp. 645–671.
[14] D. Colton and R. Kress, *Inverse Acoustic and Electromagnetic Scattering Theory*, Springer, Berlin, 1998.
[15] R. Dalang, *Extending martingale measure stochastic integral with applications to spatially homogeneous SPDEs*, Electron. J. Probab., 6 (1999), pp. 1–29.
[16] A. Devaney, *The inverse problem for random sources*, J. Math. Phys., 20 (1979), pp. 1687–1691.
[17] A. Devaney, E. Marengo, and M. Li, *Inverse source problem in nonhomogeneous background media*, SIAM J. Appl. Math., 67 (2007), pp. 1353–1378.
[18] A. Devaney and G. Sherman, *Nonuniqueness in inverse source and scattering problems*, IEEE Trans. Antennas and Propagation, 30 (1982), pp. 1034–1037.
[19] M. Eller and N. Valdivia, *Acoustic source identification using multiple frequency information*, Inverse Problems, 25 (2009), 115005.
[20] L. Evans, *An Introduction to Stochastic Differential Equations*, AMS, Providence, RI, 2013.
[21] A. Fokas, Y. Kurylev, and V. Marinakis, *The unique determination of neuronal currents in the brain via magnetoencephalogrphy*, Inverse Problems, 20 (2004), pp. 1067–1082.
[22] A. Friedman, *Stochastic Differential Equations and Applications*, Dover Publications, New York, 2006.
[23] K.-H. Hauer, L. Kühn, and R. Potthast, *On uniqueness and non-uniqueness for current reconstruction from magnetic fields*, Inverse Problems, 21 (2005), pp. 955–967.
[24] M. Hairer, *An Introduction to Stochastic PDEs*, arXiv:0907.4178, 2009.
[25] V. Isakov, *Inverse Source Problems*, AMS, Providence, RI, 1989.
[26] J. Kaipio and E. Somersalo, *Statistical and Computational Inverse Problems*, Springer-Varlag, New York, 2005.
[27] P. Li, *An inverse random source scattering problem in inhomogeneous media*, Inverse Problems, 27 (2011), 035004.
[28] E. Marengo and A. Devaney, *The inverse source problem of electromagnetics: Linear inversion formulation and minimum energy solution*, IEEE Trans. Antennas and Propagation, 47 (1999), pp. 410–412.
[29] F. Natterer, *The Mathematics of Computerized Tomography*, Teubner, Stuttgart, 1986.
[30] J. Nolen and G. Papanicolaou, *Fine scale uncertainty in parameter estimation for elliptic equations*, Inverse Problems, 25 (2009), 115021.
[31] J. Walsh, *An Introduction to Stochastic Partial Differential Equations*, Springer, Berlin, 1986.
[32] R. Yuste, *Fluorescence microscopy today*, Nat. Methods, 2 (2005), pp. 902–904.
[33] D. Zhang and Y. Guo, *Fourier method for solving the multi-frequency inverse acoustic source problem for the Helmholtz equation*, Inverse Problems, 31 (2015), 035007.